



Synthesis and characterization of novel chromone Schiff base complexes as p53 activators

Mohamad M.E. Shakhofa^{1,2} | Hanan A. Mousa² | Ammar A. Labib² |
Amira S. Abd-El-All³ | Ahmed A. El-Beih³ | Mohamed M. Abdalla⁴

¹Department of Chemistry, Faculty of Science and Arts, Khulais, University of Jeddah, Saudi Arabia

²Inorganic Chemistry Department, National Research Center, El-bohouth Street, Dokki, Cairo 12622, Egypt

³Division of Pharmaceutical and Drug Industries, Department Chemistry of Natural and Microbial Products, National Research Centre, Dokki, Cairo 12622, Egypt

⁴Research Unit, Saco Pharm. Co., 6th October City 11632, Egypt

Correspondence

Mohamad M. E. Shakhofa, Department of Chemistry, Faculty of Science and Arts, Khulais, University of Jeddah, Saudi Arabia.

Email: mshakhofa@gmail.com

A series of chromone Schiff base complexes were prepared and analytically as well as spectroscopically characterized. The ligand was found to act as a mono-basic tridentate ligand bonded covalently or coordinatively to the metal ion via deprotonated hydroxyl group, azomethine nitrogen atom and carbonyl oxygen atom of antipyrine moiety. Both electronic spectra and magnetic measurements indicated an octahedral or a distorted octahedral geometry around the metal ions for all metal complexes except the nickel complex, which had a tetrahedral geometry. In addition, the ability of the newly prepared compounds to activate the tumour suppressor p53 in cancer cells was studied, with zinc and copper complexes showing promising activities for p53 ubiquitination compared with diphenylimidazole (reference drug).

KEYWORDS

benzopyrone, metal complexes, p53, Schiff base, ubiquitin ligase

1 | INTRODUCTION

Natural and synthetic compounds containing a chromone moiety have significant biological activities, including anticancer,^[1–3] antimicrobial,^[4] antibacterial,^[5,6] antitumour,^[7] anti-inflammatory,^[8–10] anti-HIV^[11] and antioxidant^[12,13] activities. Such a moiety is also used in a wide variety of pharmacologically active compounds such as antispasmodics, for bile duct, gall bladder, relief of spasms of the ureter and bronchial asthma.^[14]

4-Aminoantipyrine is known to have a variety of medical applications as an antimicrobial,^[15–18] anti-cancer,^[16,19–21] anti-inflammatory, analgesic, antipyretic and antioxidant agent.^[22–26] It also has the ability to inhibit the cyclooxygenase isoenzymes, prostaglandin synthesis and platelet thromboxane synthesis.^[27]

From a previous interest in the biological activity of both chromone and antipyrine moieties and in

continuation of our effort to synthesize bioactive metal complexes,^[28–33] our goal in the work reported here was the preparation of a novel chromone Schiff base ligand and its complexes, and then to study the structure of the prepared compounds through elemental analysis and spectroscopic data. Moreover, we also studied the ability of these novel compounds to activate the tumour suppressor p53 in cancer cells.

2 | EXPERIMENTAL

2.1 | Materials

All the reagents employed for the preparation of the ligand and its complexes were of synthetic grade and used without further purification. All other chemicals and reagents used in this biological study were of

analytical grade and purchased from Sigma-Aldrich (St Louis, MO, USA).

2.2 | Physical Measurements

The amounts of C, H and N in the ligand and its metal complexes were evaluated at the Microanalytical Laboratory, Cairo University, Egypt. Infrared (IR) spectra of the ligand and its metal complexes were measured using KBr discs with a Jasco FT/IR 300E Fourier transform infrared spectrophotometer covering the range 400–4000 cm^{-1} . Electronic spectra in the range 200–1100 nm were recorded with a Shimadzu 2600 spectrophotometer. Thermogravimetric analysis (TGA) was carried out with a Shimadzu DT-50 thermal analyser from room temperature to 800 °C at a heating rate of 10 °C min^{-1} . Magnetic susceptibilities were measured at 25 °C using the Gouy method with mercuric tetrathiocyanatocobaltate(II) as magnetic susceptibility standard. Diamagnetic corrections were estimated from Pascal's constant.^[34] The magnetic moments were calculated from the equation: $\mu_{\text{eff}} = 2.84\sqrt{\chi_{\text{M}}^{\text{corr}}T}$. Molar conductances were measured with a Tacussel-type CD_6NG conductivity bridge using 10^{-3} M dimethylformamide (DMF) solutions. NMR spectra were obtained with a Bruker Avance 600-DRX spectrometer. The mass spectrum of the ligand was obtained using a Thermo Scientific Trace GC Ultra/ISQ single quadrupole instrument. TLC was used to confirm the purity of the compounds.

2.3 | Synthesis of Ligand

The chromone Schiff base ligand was prepared by refluxing equimolar amounts of 6-formyl-7-hydroxy-5-methoxy-2-methylbenzopyran-4-one (234 mg, 1.0 mmol) and 4-amino-1,5-dimethyl-2-phenyl-1,2-dihydro-3H-pyrazol-3-one (203 mg, 1.0 mmol) in 100 ml of hot methanol (60 °C) in the presence of three drops of glacial acetic. The mixture was refluxed for 5 h, and then the solvent evaporated to 50 ml. The solid product was filtered off, washed with cold methanol, crystallized from ethanol and dried in an oven (60 °C) for 4 h. Yield 3.45 mg (82%); dark yellow colour; m.p. 240 °C. Elemental analysis for $\text{C}_{23}\text{H}_{21}\text{N}_3\text{O}_5$ (419.44) (%): found (calcd): C, 65.41 (65.86); H, 4.88 (5.05); N, 9.81 (10.02). IR (KBr, cm^{-1}): 3500 $\nu(\text{OH})$, 1662 $\nu(\text{C}=\text{O}^{30})$, 1640 $\nu(\text{C}=\text{O}^{18})$, 1599 $\nu(\text{C}=\text{N})$, 1307 $\nu(\text{C}=\text{OH})$. ^1H NMR (600 MHz, $\text{DMSO}-d_6$, δ , ppm): 14.915 (s, 1H, $^{28}\text{O}-\text{H}$), 9.98 (s, 1H, $\text{N}-^{12}\text{C}-\text{H}$), 6.73 (s, 1H, $^7\text{C}-\text{H}$), 2.29 (s, 3H, $^1\text{C}-^{31}\text{CH}_3$), 6.03 (s, 1H, $^2\text{C}-\text{H}$), 2.41 (s, 3H, $^{14}\text{C}-^{21}\text{CH}_3$), 3.31 (s, 3H, $\text{N}-^{19}\text{CH}_3$), 3.81 (s, 3H, $\text{O}-^{29}\text{CH}_3$), 6.73 (d, 2H, ^{22}CH & ^{26}CH), 7.44 (t, 2H, ^{23}CH & ^{25}CH), 7.56 (t, 1H, ^{24}CH). ^{13}C NMR

(150 MHz, $\text{DMSO}-d_6$, δ , ppm): 164.59 (C1), 111.22 (C2), 150.2 (C4), 113.71 (C5), 175.61 (C6), 100.57 (C7), 159.31 (C8), 112.38 (C9), 160.94 (C10), 153.29 (C12), 110.67 (C13), 160.25 (C14), 164.91 (C17), 35.39 (C19), 134.39 (C20), 10.29 (C21), 128.04 (C22, C26), 129.74 (C23, C25), 125.79 (C24), 63.66 (C29), 19.75 (C31).

2.4 | Synthesis of Metal Complexes

The metal complexes (2–6) were prepared by adding dropwise a hot methanolic solution (50 ml, 60 °C) of 1 mmol of each of the metal salts $\text{Mn}(\text{CH}_3\text{COO})_2 \cdot 4\text{H}_2\text{O}$, $\text{Ni}(\text{CH}_3\text{COO})_2 \cdot 4\text{H}_2\text{O}$, $\text{Co}(\text{CH}_3\text{COO})_2 \cdot 4\text{H}_2\text{O}$, $\text{Cu}(\text{CH}_3\text{COO})_2 \cdot \text{H}_2\text{O}$ and $\text{Zn}(\text{CH}_3\text{COO})_2 \cdot 2\text{H}_2\text{O}$ to a hot methanolic solution (50 ml, 60 °C) of the ligand (419 mg, 1 mmol). The reaction mixture was refluxed for 3 h. The resulting precipitate was filtered off, washed with ethanol and then with diethyl ether and dried in a vacuum desiccator over P_4O_{10} .

2.4.1 | Mn complex (2)

Yield 71%; m.p. > 300 °C; colour, light brown; $\mu_{\text{eff}} = 5.88$; molar conductivity = $16.6 \Omega^{-1} \text{cm}^2 \text{mol}^{-1}$. Elemental analysis for $[\text{Mn}(\text{L})(\text{CH}_3\text{COO})(\text{H}_2\text{O})_2]$, $\text{C}_{23}\text{H}_{27}\text{N}_3\text{O}_9\text{Mn}$ (568.44) (%): found (calcd): C, 52.64 (52.82); H, 4.90 (4.79); N, 7.17 (7.39). IR (KBr, cm^{-1}), 3427 $\nu(\text{H}_2\text{O})$, 1662 $\nu(\text{C}=\text{O}^{30})$, 1625 $\nu(\text{C}=\text{O}^{18})$, 1581 $\nu(\text{C}=\text{N})$, 1314 $\nu(\text{C}-\text{OH})$, 616 $\nu(\text{Mn}-\text{O})$, 532 $\nu(\text{Mn}-\text{N})$, $\nu_{\text{s}}(\text{CH}_3\text{COO})$, $\nu_{\text{as}}(\text{CH}_3\text{COO})$ 1570, 1366 ($\Delta = 204 \text{cm}^{-1}$).

2.4.2 | Co complex (3)

Yield 58%; m.p. > 300 °C; colour, reddish brown; $\mu_{\text{eff}} = 4.05$; molar conductivity = $22.0 \Omega^{-1} \text{cm}^2 \text{mol}^{-1}$. Elemental analysis for $[\text{Co}(\text{L})(\text{CH}_3\text{COO})(\text{H}_2\text{O})_2] \cdot \text{H}_2\text{O}$, $\text{C}_{25}\text{H}_{29}\text{N}_3\text{O}_{10}\text{Co}$ (590.45) (%): found (calcd): C, 50.50 (50.86); H, 4.50 (4.95); N, 7.60 (7.12). IR (KBr, cm^{-1}), 3390 $\nu(\text{H}_2\text{O})$, 1655 $\nu(\text{C}=\text{O}^{30})$, 1623 $\nu(\text{C}=\text{O}^{18})$, 1571 $\nu(\text{C}=\text{N})$, 1330 $\nu(\text{C}-\text{OH})$, 507 $\nu(\text{Co}-\text{O})$, 463 $\nu(\text{Co}-\text{N})$, $\nu_{\text{s}}(\text{CH}_3\text{COO})$, $\nu_{\text{as}}(\text{CH}_3\text{COO})$ 1531, 1363 ($\Delta = 208 \text{cm}^{-1}$).

2.4.3 | Ni complex (4)

Yield 64%; m.p. > 300 °C; colour, brown; $\mu_{\text{eff}} = 2.62$; molar conductivity = $15.0 \Omega^{-1} \text{cm}^2 \text{mol}^{-1}$. Elemental analysis for $[\text{Ni}(\text{L})(\text{CH}_3\text{COO})] \cdot \text{H}_2\text{O}$, $\text{C}_{25}\text{H}_{25}\text{N}_3\text{O}_8\text{Ni}$ (554.17) (%): found (calcd): C, 54.39 (54.18); H, 5.10 (4.55); N, 7.80 (7.58). IR (KBr, cm^{-1}), 3403 $\nu(\text{H}_2\text{O})$, 1670 $\nu(\text{C}=\text{O}^{30})$, 1616 $\nu(\text{C}=\text{O}^{18})$, 1576 $\nu(\text{C}=\text{N})$, 1317 $\nu(\text{C}-\text{OH})$, 585 $\nu(\text{Ni}-\text{O})$, 507 $\nu(\text{Ni}-\text{N})$, $\nu_{\text{s}}(\text{CH}_3\text{COO})$, $\nu_{\text{as}}(\text{CH}_3\text{COO})$ 1547, 1340 ($\Delta = 207 \text{cm}^{-1}$).

2.4.4 | Cu complex (5)

Yield 56%; m.p. > 300 °C; colour, brown; $\mu_{\text{eff}} = 1.33$; molar conductivity = $18.1 \Omega^{-1} \text{ cm}^2 \text{ mol}^{-1}$ Elemental analysis for $[\text{Cu}(\text{L})(\text{CH}_3\text{COO})(\text{H}_2\text{O})_2] \cdot 3\text{H}_2\text{O}$, $\text{C}_{25}\text{H}_{33}\text{N}_3\text{O}_{12}\text{Cu}$ (631.1) (%): found (calcd): C, 47.87 (47.58); H, 5.91 (5.27); N, 6.42 (6.66). IR (KBr, cm^{-1}), 3420 $\nu(\text{H}_2\text{O})$, 1658 $\nu(\text{C}=\text{O}^{30})$, 1625 $\nu(\text{C}=\text{O}^{18})$, 1588 $\nu(\text{C}=\text{N})$, 1315 $\nu(\text{C}-\text{OH})$, 590 $\nu(\text{Cu}-\text{O})$, 516 $\nu(\text{Cu}-\text{O})$, 490 $\nu(\text{Cu}-\text{N})$, $\nu_{\text{s}}(\text{CH}_3\text{COO})$, $\nu_{\text{as}}(\text{CH}_3\text{COO})$ 1570, 1390 ($\Delta = 180 \text{ cm}^{-1}$).

2.4.5 | Zn complex (6)

Yield 54%; m.p. > 300 °C; colour, beige; molar conductivity = $19.6 \Omega^{-1} \text{ cm}^2 \text{ mol}^{-1}$ Elemental analysis for $[\text{Zn}(\text{L})(\text{CH}_3\text{COO})(\text{H}_2\text{O})_2] \cdot \text{H}_2\text{O}$, $\text{C}_{23}\text{H}_{29}\text{N}_3\text{O}_{10}\text{Zn}$ (596.89) (%): found (calcd): C, 49.78 (50.31); H, 4.97 (4.90); N, 7.19 (7.04). IR (KBr, cm^{-1}), 3400 $\nu(\text{H}_2\text{O})$, 1663 $\nu(\text{C}=\text{O}^{30})$, 1608 $\nu(\text{C}=\text{O}^{18})$, 1587 $\nu(\text{C}=\text{N})$, 1313 $\nu(\text{C}-\text{OH})$, 569 $\nu(\text{Zn}-\text{O})$, 487 $\nu(\text{Zn}-\text{N})$, $\nu_{\text{s}}(\text{CH}_3\text{COO})$, $\nu_{\text{as}}(\text{CH}_3\text{COO})$ 1540, 1350 ($\Delta = 190 \text{ cm}^{-1}$).

2.5 | Biological Activity

2.5.1 | *In vitro* ubiquitination assay

The expression of recombinant glutathione-S-transferase-tagged MDM2 (GST-MDM2) was induced in 25 ml culture of exponentially growing *Escherichia coli* BL21 cells (OD₆₀₀ 0.6) by 1 mM isopropylthio-b-D-galactoside for 3 h. GST-MDM2 was purified on glutathione-sepharose beads (Amersham). The beads were washed with 50 mM Tris (pH = 7.5).

Fluorescent ubiquitin (5 μg ; Invitrogen, Malvern, PA, USA), 50 ng of mammalian E1 (Enzo, New York, NY, USA), 200 ng of human recombinant UbcH5B E2 (Enzo) and 200 ng of His-p53 (Enzo) were mixed with reaction buffer (50 mM Tris (pH 8), 2 mM dithiothreitol, 5 mM MgCl_2 , 2 mM adenosine triphosphate). A dose of each newly synthesized compound (50 ng) or dimethylsulfoxide (DMSO) was added to the mixture, which was then pipetted onto GS4b-MDM2 beads. The suspension was incubated at 37 °C, with shaking at 1200 rpm, for 1 h and then stopped by the addition of 3 \times sodium dodecylsulfate sample buffer. Free fluorescent ubiquitin was washed off, and the total fluorescent ubiquitin signal measured with a monochromator plate reader (Safre, Männedorf, Switzerland).

2.5.2 | Non-fluorescent *in vitro* ubiquitination assays

The procedure was as above except that 5 μg of unlabelled ubiquitin (Enzo) was used. An amount of 10 μl of each test compound or DMSO was added to the mixture and

pipetted onto GS4b-MDM2 beads. After incubation, as described above, reaction products were resolved using sodium dodecylsulfate-polyacrylamide gel electrophoresis (SDS-PAGE) and analysed by Western blotting with anti p53 DO-1. For the MDM2 auto-ubiquitination assay, GS4b-MDM2 RING beads were prepared as above and used in place of the full length MDM2.

2.5.3 | *In vivo* ubiquitination of p53

H1299 cells (p53-null human non-small-cell lung adenocarcinoma cells) were obtained from the American Type Culture Collection (ATCC; Manassas, VA, USA) and cultured in Dulbecco's modified Eagle's medium (DMEM; Invitrogen), supplemented with 10% foetal calf serum, 1% L-glutamine, 50 U ml^{-1} penicillin G and 50 $\mu\text{g ml}^{-1}$ streptomycin sulfate at 37 °C and 5% CO_2 .

Retinal pigment epithelial cells were obtained from ATCC and cultured in DMEM/F12 HAM (Invitrogen), supplemented with 10% foetal calf serum, 1.6% sodium bicarbonate, 1% L-glutamine, 50 U ml^{-1} penicillin G and 50 $\mu\text{g ml}^{-1}$ streptomycin sulfate at 37 °C and 5% CO_2 .

U2OS-GFP-MDM2 TetOn cells were made by transfecting a U2OS TetOn cell line with a pTRE2 GFP-MDM2 plasmid and pBabe Eco Puro plasmid. Cells were selected for 2 weeks using puromycin. Colonies resistant to puromycin would pick and grow in DMEM with supplements. Several clones were tested using fluorescence microscopy to ensure that GFP (green fluorescent protein) positive nuclei were visible after doxocycline induction and tested for inducible GFP-MDM2 expression by Western blotting. Clone 2 was selected for further work. RKO cells (wild-type and null for p53; obtained from ATCC and authenticated by short-tandem repeat profiling/karyotyping/isoenzyme analysis) were a gift from Dr Bert Vogelstein (Sidney Kimmel Comprehensive Cancer Center, Baltimore, MD, USA) and were cultured in DMEM with supplements and under conditions as described above.

Cells were transfected with GeneJuice (Merck, Darmstadt, Germany) according to the manufacturer's instructions. Cells were treated with 10 μM Nutlin-3a (Roche) and the newly synthesized test compound at the indicated doses. The plasmid expressing human wild-type p53 has been described previously.^[35] Wild-type MDM2 has been described previously.^[36]

Dr R. Hay (Centre for Gene Regulation and Expression, College of Life Sciences, University of Dundee, UK) kindly provided HA-tagged ubiquitin (Boston Biochem, Cambridge, MA, USA). The GFP-MDM2 plasmid used to make the U2OS GFP-MDM2 TetOn cell line described above was cloned from pEGFPC1 MDM2 (wild-type MDM2 cloned into Clontec backbone) into the pTRE2 plasmid (Clontech, Mountain View, CA, USA).

Cells were grown in DMEM with 10% (v/v) foetal bovine serum and seeded in 10 cm plates to reach 50% confluence 24 h prior to transfection with 1 μg of p53, 4 μg of MDM2 and 1 μg of HIS-ubiquitin with 1.5 μl of GeneJuice reagent (Merck). After 20 h, cells treated with the newly synthesized compounds for 6 h, and MG132 (Sigma Aldrich) for 4 h were washed and collected in phosphate-buffered saline. The remaining cells were centrifuged for 5 min at 5000 g and the cell pellet lysed in 700 μl of ubiquitin buffer A (6 M guanidinium HCl, 300 mM NaCl, 50 mM phosphate (pH = 8.0), 100 $\mu\text{g ml}^{-1}$ *N*-ethylmaleimide) and sonicated for 5 min at 20% amplitude (Fisher sonicator model 500). Lysates were incubated overnight with Invitrogen Dynabeads His-Tag matrix, and washed once with each of the ubiquitin buffers A, B and C, and finally phosphate-buffered saline (ubiquitin buffer B: mixture of ubiquitin buffers A and C 1:1 (v/v); ubiquitin buffer C: 300 mM NaCl, 50 mM phosphate (pH = 8.0), 100 $\mu\text{g ml}^{-1}$ *N*-ethylmaleimide). Adsorbed proteins were resolved by 8% SDS-PAGE, followed by immunoblotting with a p53 (DO-1) antibody (Sigma Aldrich).

3 | RESULTS AND DISCUSSION

A new chromone Schiff base ligand (**1**) was prepared through the reaction of 4-aminoantipyrine and 6-formyl-7-hydroxy-5-methoxy-2-methylbenzopyran-4-one (Figure 1). Ligand **1** reacted with acetate salts of Cu(II), Co(II), Ni(II), Mn(II) and Zn(II) in equal molar ratio. The physical data of complexes **2–6** showed that they are coloured, stable in air and dissolve only in DMSO or DMF. The spectral and analytical data are in agreement with the suggested structures for metal complexes **2–6** (Figures 2 and 3).

3.1 | IR Spectra

The IR spectrum of the ligand displayed strong to medium peaks at 3500, 1662, 1640, 1599 and 1307 cm^{-1} , ascribed to

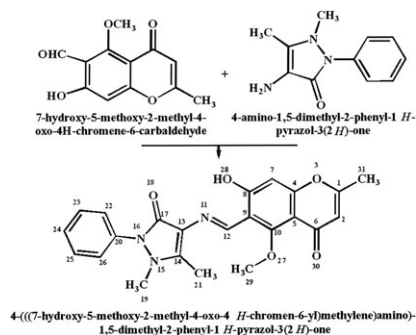


FIGURE 1 Synthesis of chromone Schiff base ligand **1**

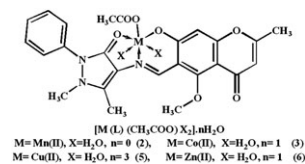


FIGURE 2 Proposed structures of chromone Schiff base complexes **2**, **3**, **5** and **6**

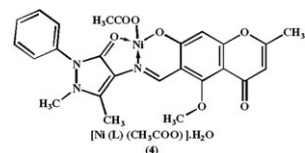


FIGURE 3 Proposed structure of chromone Schiff base nickel(II) complex **4**

the phenolic $\nu(\text{OH})$ stretching vibration, carbonyl groups of benzopyrone and antipyrine moieties, azomethine group and phenolic C—O stretching, respectively.^[37–41] The bonding behaviour of the ligand was established from comparing the IR spectra of both parent ligand and its complexes. This comparison showed that the ligand acts as a monobasic tridentate agent bonding with metal ions through carbonyl oxygen atom of antipyrine moiety, azomethine nitrogen atom and deprotonated hydroxyl group. The following evidence suggests this bonding mode:

- The disappearance of phenolic $\nu(\text{OH})$ band with higher shift of phenolic C—O band appearing in the 1313–1330 cm^{-1} range.
- The band characteristic of antipyrine moiety carbonyl group shifted to shorter wavenumber and appeared in the 1608–1625 cm^{-1} range.^[42]
- The band characteristic of the azomethine group shifted to shorter wavenumber and appeared in the 1571–1588 cm^{-1} range that is consistent with that reported by El-Sawaf *et al.*^[43] and El-Tabl.^[44]
- The presence of new bands in the 461–616 cm^{-1} range could be attributed to the metal bond with oxygen and nitrogen atoms.
- The presence of two bands in the 1531–1570 and 1340–1390 cm^{-1} ranges were attributed to $\nu_a(\text{COO}^-)$ and $\nu_s(\text{COO}^-)$, respectively. The separation between these peaks equals 180–208 cm^{-1} , which indicates that the acetate ions act as a monodentate ligand towards the metal ions.^[45] A broad band around 3390–3480 cm^{-1} corresponds to the existence of coordinated or hydrated water molecules in these complexes.

3.2 | NMR Spectra

3.2.1 | ^1H NMR spectra

The ^1H NMR spectrum of the ligand in $\text{DMSO-}d_6$ (Figure 4) is in agreement with the proposed structure (Figure 1). The singlets at 14.92 and 9.98 ppm were ascribed to the proton of hydroxyl group (s, 1H, $^8\text{C}-^{28}\text{OH}$) and proton of azomethine group (s, 1H, $\text{N}=\text{C}^{\text{H}}$), respectively.^[41] The hydrogen chemical shifts of hydroxyl group were observed at high δ values because of its attachment to highly electronegative atom (oxygen). This conclusion was confirmed by the ligand spectrum in the presence of one drop of D_2O , in which the intensity of this signal is markedly reduced (Figure 5). The chemical shifts observed as singlets at 6.73 ppm (s, 1H, ^7CH) and 6.03 ppm (s, 1H, ^2CH) could be ascribed to the protons of benzopyrone moiety.^[37,38] While the signals at 2.29 ppm (s, 3H, $^{31}\text{CH}_3$) and 3.81 ppm (s, 3H, $\text{O}-^{29}\text{CH}_3$) could be ascribed to the protons of methyl and methoxy groups attached to benzopyrone moiety.^[39] The aromatic protons of antipyryne moiety appeared at 6.73–7.56 ppm. The singlets that appeared at 2.41 ppm (s, 1H, $\text{C}-^{21}\text{CH}$) and 3.31 ppm (s, 1H, $\text{N}-^{19}\text{CH}_3$) were attributed to the protons of methyl groups of antipyryne moiety.^[46]

3.2.2 | ^{13}C NMR spectra

The ^{13}C NMR spectrum of the ligand in $\text{DMSO-}d_6$ (Figure 6) showed signals at 175.61 and 164.91 ppm which may be attributed to carbon atoms of carbonyl groups of benzopyrone ($^6\text{C}=\text{O}$) and antipyryne ($^{17}\text{C}=\text{O}$) moieties, respectively.^[38,39] The signal of azomethine carbon ($^{12}\text{C}=\text{N}$) was observed at 153.29 ppm, while other carbons

of benzopyrone moiety are slightly shifted.^[41] The peaks appearing at 63.66 and 19.75 ppm could be owing to methoxy and methyl carbon atoms of benzopyrone moiety ($^{29}\text{CH}_3-\text{O}$ and $^{31}\text{CH}_3-\text{C}$)^[37,41] while signals in the 125.79–129.74 ppm range belong to aromatic carbons of antipyryne moiety. The signals at 10.29 and 35.39 ppm are due to methyl groups of antipyryne moiety, whereas the signals at 110.67 and 160.25 are due to the carbon atoms of pyrazol ring (C^{13} and C^{14}). Detailed analysis using 1D-NMR (^1H , ^{13}C) DEPT (90, 135) revealed that the ligand has four CH_3 , eight CH and eleven quaternary carbon atoms.

3.2.3 | 2D-NMR spectra

The HSQC spectrum of the ligand was recorded and used to assign the signals unambiguously (Figure 7). The observed correlations in the HSQC spectrum were attributed to the signals for carbons containing hydrogen only. The ^1H NMR singlet signals observed at 6.03, 6.73 and 2.29 ppm showed a relation with the carbon atoms of benzopyrone moiety at 111.22, 100.57 and 19.75 ppm. Hence, the first and second signal must be due to protons of benzopyrone moiety while the last signal must be due to the methyl group ($^{31}\text{CH}_3-\text{C}$) of benzopyrone. The signals appearing at 7.40, 7.43 and 7.56 ppm, assigned to H^{24} , $\text{H}^{22,26}$ and $\text{H}^{23,25}$, displayed a relation with the three carbon atoms at 125.79, 128.04 and 129.74 ppm, respectively. From the previous correlations, we can deduce that these protons can be attributed to the aromatic protons of antipyryne moiety. In addition, the proton signals appearing at 3.31 and 2.41 ppm showed a relation with the carbon signals at 35.39 and 10.29 ppm; hence, they are due to the methyl carbon of antipyryne moiety.

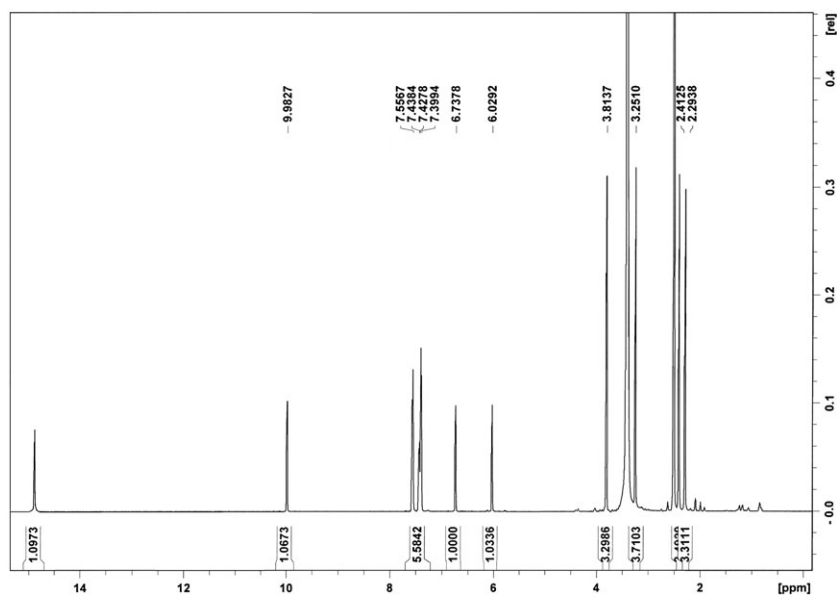


FIGURE 4 ^1H NMR spectrum of chromone Schiff base ligand **1**

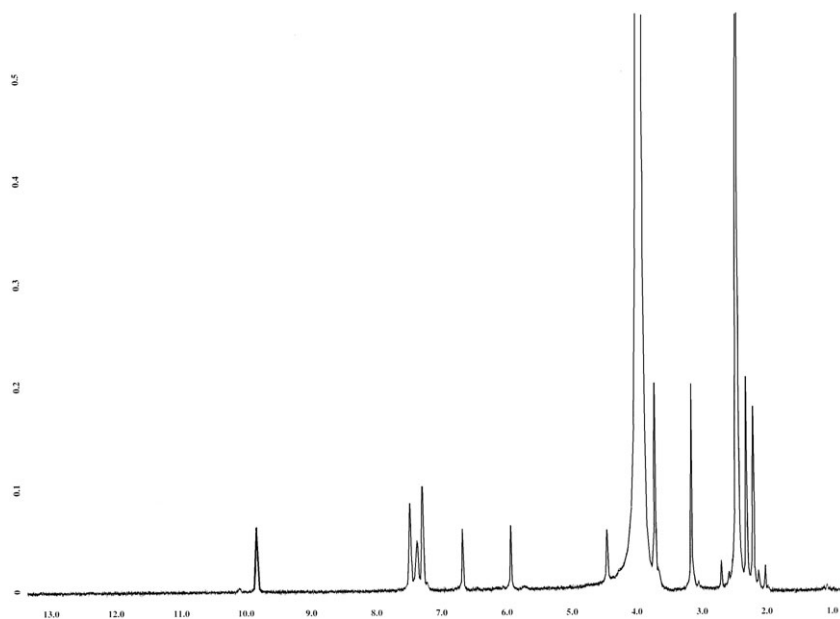


FIGURE 5 ^1H NMR spectrum of chromone Schiff base ligand **1** (one drop of D_2O)

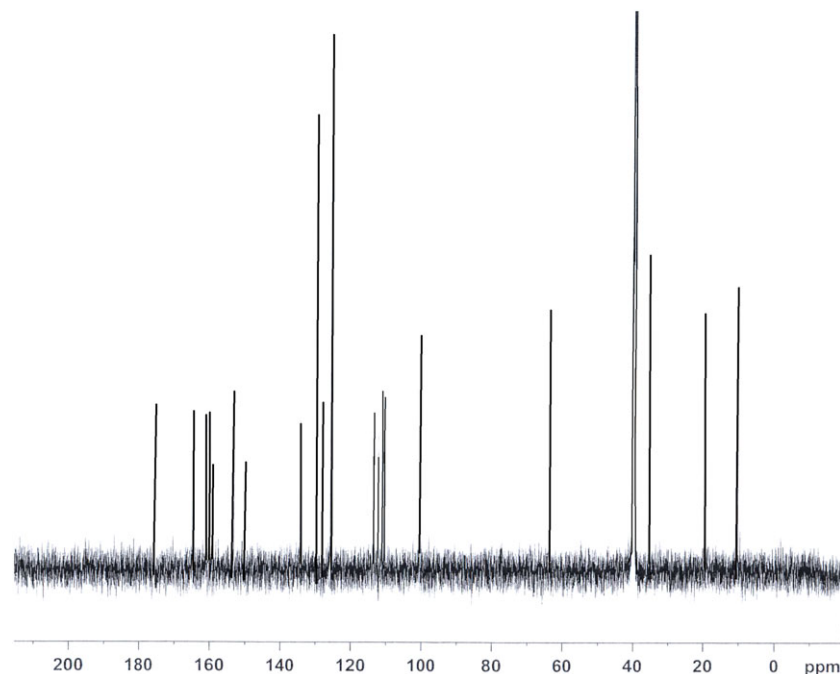


FIGURE 6 ^{13}C NMR spectrum of chromone Schiff base ligand **1**

3.3 | Mass Spectra

The mass spectrum of ligand **1** supports the proposed structure with the molecular ion peak m/z at 419. Furthermore, six fragments can be elucidated. The peak at m/z 405 belongs to the fragment ($\text{C}_{22}\text{H}_{19}\text{N}_3\text{O}_5$) due to the loss of methyl group of the methoxy moiety. The peaks at m/z 327 and 313 belong to the fragments ($\text{C}_{17}\text{H}_{17}\text{N}_3\text{O}_4$) and ($\text{C}_{16}\text{H}_{15}\text{N}_3\text{O}_4$) which are due to loss of benzene ring and hydroxyl group consequently loss of methyl group of antipyrine moiety. The peaks at $m/z = 203, 218, 84$ and 78 refer to the fragments ($\text{C}_{11}\text{H}_{13}\text{N}_3\text{O}$, 4-amino-1,5-dimethyl-2-phenyl-1,2-dihydro-

3*H*-pyrazol-3-one), ($\text{C}_{12}\text{H}_{10}\text{O}_4$, 5-methoxy-2-methyl-6-methylene-4*H*-chromene-4,7(6*H*)-dione), ($\text{C}_3\text{H}_4\text{N}_2\text{O}$, 1,2-dihydro-3*H*-pyrazol-3-one) and (C_6H_6), respectively (Figure 8).

3.4 | Molar Conductance Measurements

The molar conductivity of complexes **2–6** was measured at a concentration of 0.001 M in DMSO. All complexes show molar conductivity values between 15 and 22 $\Omega^{-1} \text{cm}^2 \text{mol}^{-1}$, which are within the expected range for non-electrolytes.^[47] These data indicate the absence of

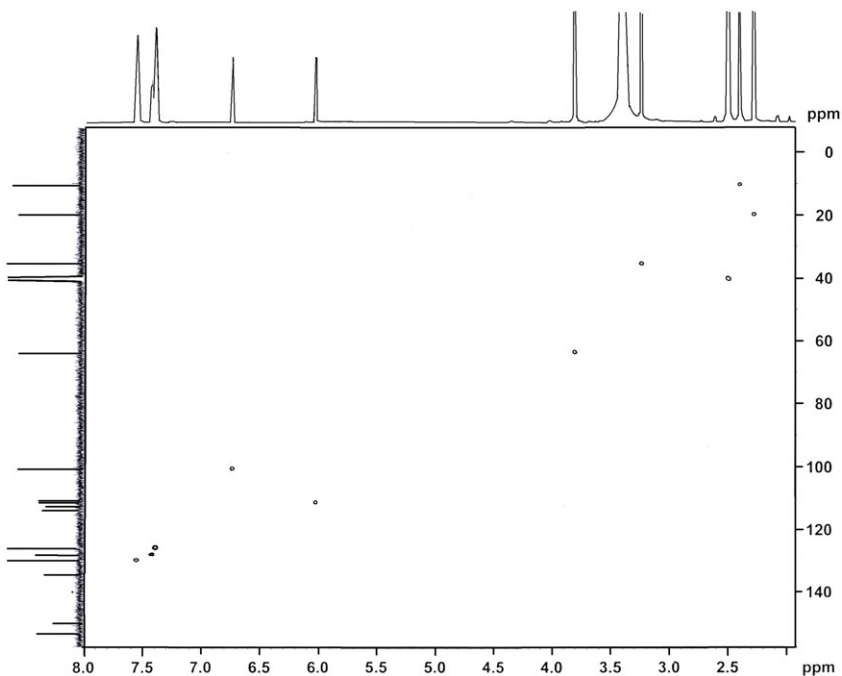


FIGURE 7 HSQC spectrum of chromone Schiff base ligand **1**

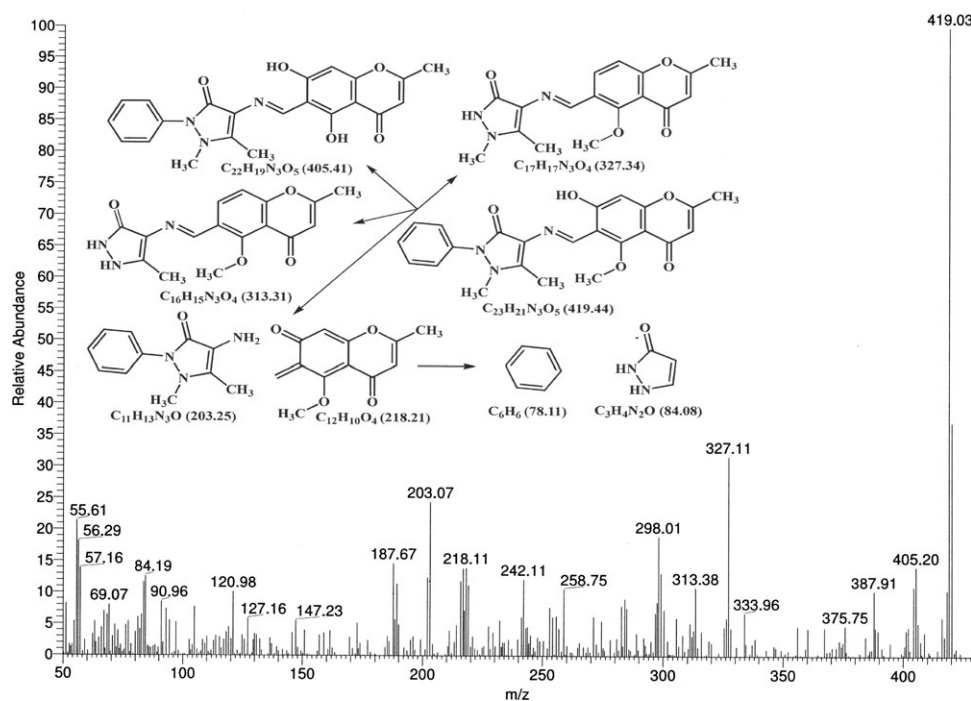


FIGURE 8 Mass spectrum and fragmentation pattern of chromone Schiff base ligand **1**

any acetate ions outside the coordination sphere of all the complexes. The partial solvolysis by solvent molecules could explain the high values for some of the complexes.

3.5 | Electronic Spectra and Magnetic Moments

The electronic absorption spectra of compounds **1–6** recorded in DMSO are illustrated in Figures 9 and 10

and data summarized in Table 1. The ligand spectrum exhibits four bands at 270, 288, 340 and 380 nm. The first two bands are due to $\pi \rightarrow \pi^*$ transitions of the benzenoid and benzopyrone moieties, which are nearly unchanged by complexation. The third and fourth bands result from $n \rightarrow \pi^*$ and charge transfer transitions of both azomethine and carbonyl groups. The shifts in these bands are evidence for the participation of these groups ($C=O$, $C=N$) in coordination with metal ions.^[48] In

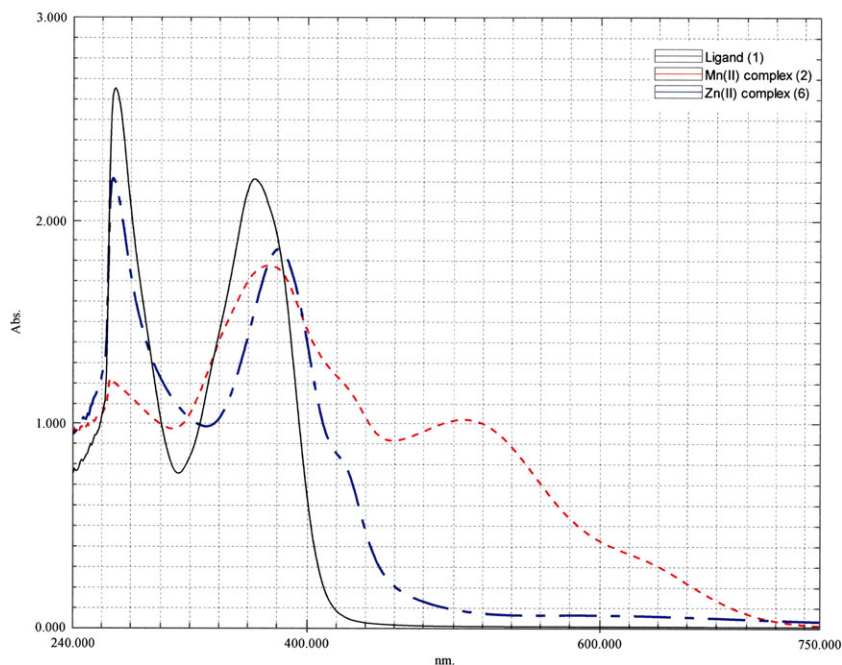


FIGURE 9 UV-visible spectra of ligand and Mn(II) and Zn(II) complexes

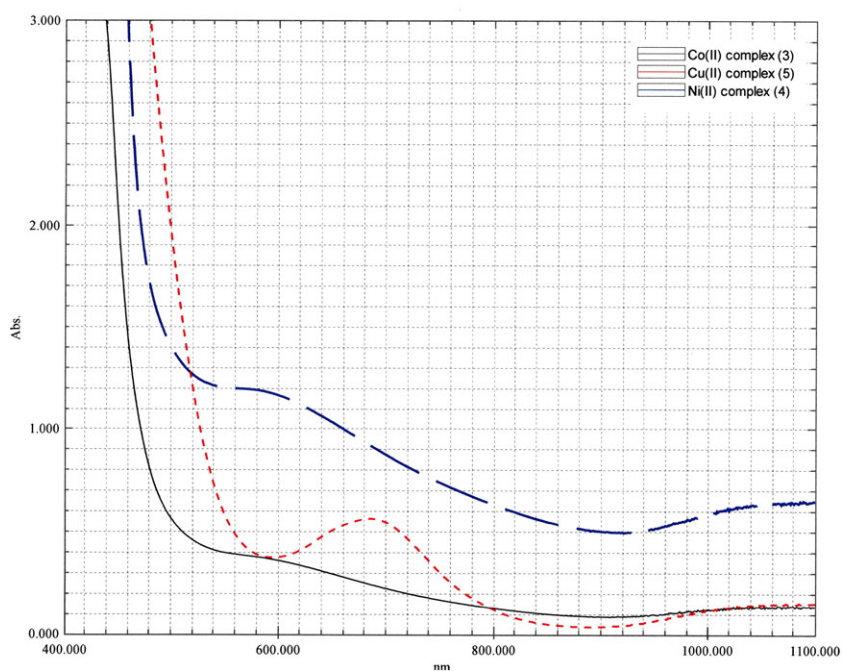


FIGURE 10 UV-visible spectra of Co(II), Ni(II) and Cu(II) complexes

addition, new absorption bands appeared between 400 and 435 nm in the spectra of the complexes, which may be assigned to the ligand-to-metal charge transfer transitions.

Complex 2 shows a magnetic moment value of 5.93 BM and weak absorption bands at 635, 520 and 440 nm assignable to ${}^6A_{1g} \rightarrow {}^4T_{1g}(4G)(\nu_1)$, ${}^6A_{1g} \rightarrow {}^4E_g(4G)(\nu_2)$ and ${}^6A_{1g} \rightarrow {}^4E_g(4D)(\nu_3)$ transitions, respectively. Both magnetic moment value and absorption spectrum of this complex well match an octahedral geometry around the Mn(II) ion.^[48] Complex 3 shows a magnetic moment

value of 3.95 BM and two absorption bands at 1055 and 580 nm, corresponding to ${}^4T_{1g}(F) \rightarrow {}^4T_{2g}(F)$ and ${}^4T_{1g}(F) \rightarrow {}^4A_{2g}(F)$ transitions, respectively. These results suggest an octahedral geometry structure for that complex.^[48–52] The ratio of ν_1/ν_2 is 1.82, lower than for octahedral Co(II) (1.95–2.48), indicating a distorted octahedral structure. This is consistent with the band broadness that could be attributed to the envelope of the transitions from ${}^4E_g({}^4T_{1g})$ to the components ${}^4B_{2g}$ and 4E_g of ${}^4T_{2g}$, characteristic of a tetragonal distorted octahedral environment.^[48–52] The third band which is assigned to (ν_3)

TABLE 1 UV-visible spectral data and magnetic moments for the ligand and its complexes

Compound	π - π^* , n - π^* , charge transfer and d-d bands	d-d transition	Geometry	μ_{eff} (BM)
1	270, 288, 340, 380			-
2	265, 290, 355, 380, 400, 440, 520, 635	${}^6A_{1g} \rightarrow {}^4T_{1g}(4G)(\nu_1)$ ${}^6A_{1g} \rightarrow {}^4E_g(4G)(\nu_2)$ ${}^6A_{1g} \rightarrow {}^4E_g(4D)(\nu_3)$	Octahedral	5.93
3	270, 285, 360, 490, 435, 580, 1045	${}^4T_{1g}(F) \rightarrow {}^4T_{2g}(F)$ ${}^4T_{1g}(F) \rightarrow {}^4A_{2g}(F)$	distorted octahedral	3.95
4	267, 290, 350, 420, 570, 1056	${}^3A_2(F) \leftarrow {}^3T_1(F)$ ${}^3T_1(P) \leftarrow {}^3T_1(F)$	Tetrahedral	3.03
5	270, 290, 355, 410, 430, 680, 1090	$(\nu_1)^2B_{1g} \rightarrow {}^2A_{1g} (d_{x^2-y^2} \rightarrow d_{z^2})$ $(\nu_2)^2B_{1g} \rightarrow {}^2B_{2g} (d_{x^2-y^2} \rightarrow d_{xy})$	Tetragonal distorted octahedral	1.56
6	270, 285, 370, 400, 425	—		Diamagnetic

${}^4T_{1g}(F) \rightarrow {}^4T_{1g}(P)$ does not appear here, which may be due to band broadening. Complex **4** displays two absorption bands located at 1056 and 570 nm attributed to ${}^3A_2(F) \leftarrow {}^3T_1(F)$ and ${}^3T_1(P) \leftarrow {}^3T_1(F)$ transitions, respectively. The observed magnetic moment of this complex is 3.03 BM. These results are consistent with a tetrahedral geometry structure for the Ni(II) complex.^[48,53] Complex **5** exhibits two absorption bands at 1090 and 680 nm, which are due to the $(\nu_1)^2B_{1g} \rightarrow {}^2A_{1g} (d_{x^2-y^2} \rightarrow d_{z^2})$ and $(\nu_2)^2B_{1g} \rightarrow {}^2B_{2g} (d_{x^2-y^2} \rightarrow d_{xy})$ transitions. The position of these bands as well as the magnetic moment value (1.56 BM) confirmed a tetragonal distorted octahedral geometry for this complex.^[48,54–56] The third band which is assigned to $(\nu_3)^2B_{1g} \rightarrow {}^2E_g (d_{x^2-y^2} \rightarrow d_{xy})$ does not appear here which may be due to the broadening of the bands. The diamagnetic zinc complex **6** has a d^{10} system, so it

does not show d-d transitions. The peak that is observed may be because of intra-ligand transitions.^[48,57]

3.6 | Thermal Studies

TGA of complexes **2–6** was conducted in the range 20–800 °C, and the resulting data are presented in Table 2. Thermogravimetric behaviour of complex **2** (Figure 11) and complex **4** suggests three prominent steps for weight loss. The first stage for complex **2** shows a weight loss of 6.08% (calcd 6.33%) which occurs in the range 140–195 °C, equivalent to the removal of two coordinated water molecules. Whereas, the first stage for complex **4** occurs at 60–85 °C with weight loss of 2.98% (calcd 3.24%), matching with exclusion of one hydrated water molecule. The second stage of decomposition at

TABLE 2 TGA data of chromene Schiff base complexes **2–6**

Complex	Temp. range (°C)	Loss in weight: found (calcd)	Assignment	Composition of residue
2	140–195	6.08 (6.33)	Loss of coordinated water molecule	[Mn(L)(CH ₃ COO)]
	200–220	9.96 (10.37)	Loss of one acetate ion (CH ₃ COOH)	[Mn(L)]
	450–530	71.98 (73.62)	Complex decomposition forming MnO	MnO
3	55–80	2.79 (3.04)	Dehydration process (H ₂ O)	[Co(L)(CH ₃ COO)·(H ₂ O) ₂]
	110–170	5.88 (6.09)	Loss of coordinated water molecule	[Co(L)(CH ₃ COO)]
	240–275	9.28 (9.99)	Loss of one acetate ion (CH ₃ COOH)	[Co(L)]
	405–550	69.17 (70.87)	Complex decomposition forming CoO	CoO
4	60–85	2.98 (3.24)	Dehydration process (H ₂ O)	[Ni(L)(CH ₃ COO)]
	245–275	10.43 (10.64)	Loss of one acetate ion (CH ₃ COOH)	[Ni(L)]
	470–570	74.12 (75.51)	Complex decomposition forming NiO	NiO
5	75–90	8.13 (8.55)	Dehydration process (3H ₂ O)	[Cu(L)(CH ₃ COO)(H ₂ O) ₂]
	120–180	5.21 (5.70)	Loss of coordinated water molecule	[Cu(L)(CH ₃ COO)]
	180–250	9.08 (9.34)	Loss of one acetate ion (CH ₃ COOH)	[Cu(L)]
	350–750	64.97 (66.31)	Complex decomposition forming CuO	CuO
6	55–80	2.89 (3.02)	Dehydration process (H ₂ O)	[Zn(L)(CH ₃ COO)(H ₂ O) ₂]
	115–165	5.78 (6.03)	Loss of coordinated water molecule	[Zn(L)(CH ₃ COO)]
	190–230	9.21 (9.88)	Loss of one acetate ion (CH ₃ COOH)	[Zn(L)]
	425–535	68.76 (70.11)	Complex decomposition forming ZnO	ZnO

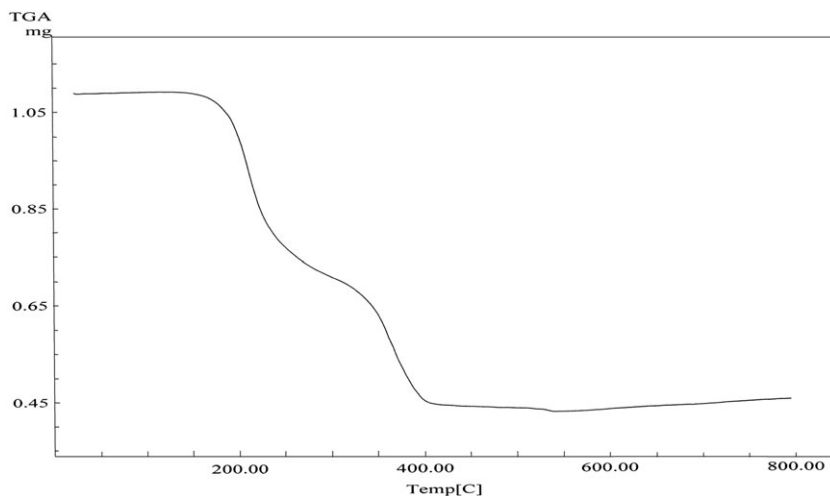


FIGURE 11 TGA curve of Mn(II) complex

200–275 °C with weight loss of 10.43 and 9.96% (calcd 10.64 and 10.37%), respectively, is consistent with removal of one acetate ion. The last step of decomposition of these complexes (**2** and **4**) occurs at 450–570 °C with weight loss of 74.12 and 71.98% (calcd 75.51 and 73.62%), respectively, which may be indicative of complete decomposition of the complex molecules leaving metal oxide as residue. In contrast, complexes **3**, **5** (Figure 12) and **6** show weight loss in four prominent steps. The first stage takes place at 55–90 °C with weight loss of 2.79, 8.13 and 2.89% (calcd 3.04, 8.55 and 3.02%), respectively, corresponding to loss of three or one hydrated water molecules. The weight loss in the second step is 5.88, 5.21 and 5.78% (calcd 6.09, 5.70 and 6.03%), respectively, that occurs at 110–180 °C corresponding to the removal of two coordinated water molecules. These complexes show a third stage of decomposition between 190 and 280 °C with weight loss of 9.28, 9.08 and 9.21% (calcd 9.99, 9.34 and 9.88%), respectively, is which due to the elimination of one acetate ion. The last step of decomposition occurs at 425–565 °C corresponding to

the complete decomposition of the complex molecules leaving metal oxide.

3.7 | Biological Activity

Due to the important role of the tumour suppressor protein p53 in preventing cancer through protecting cells from malignant transformation, we were interested in investigating the capability of the newly prepared compounds **1–6** for inhibition of p53 ubiquitination. One of the most successful strategies for promoting that inhibition is by inhibiting the interaction between p53 and MDM2, where MDM2 blocks the ability of p53 to activate transcription.^[58] The IC₅₀ of p53 ubiquitination was evaluated for compounds **1–6**, according to the methodology described in Section 2.^[59–62] The results presented in Table 3 indicate that most of the compounds show strong *in vitro* and *in vivo* inhibition of p53 ubiquitination. Among these compounds, copper and zinc complexes (**5** and **6**), which disrupt the p53–MDM2 binding with IC₅₀ values of 0.21 and 0.16 μM, appear to show the most

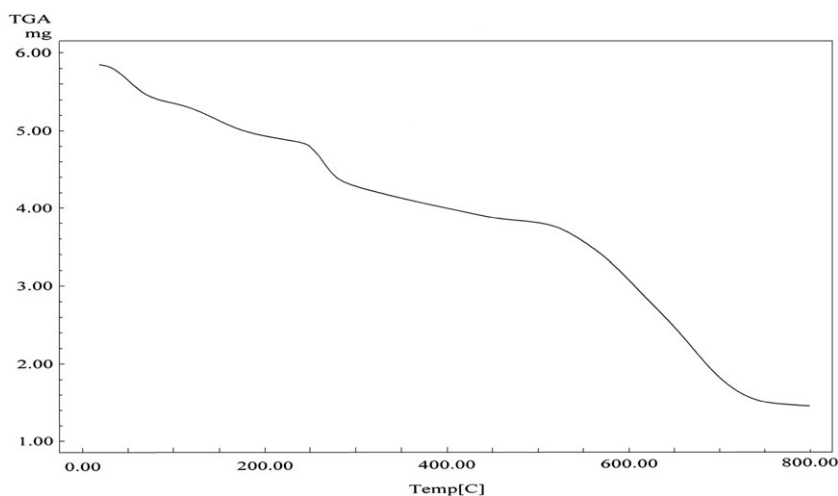


FIGURE 12 TGA curve of Cu(II) complex

TABLE 3 IC₅₀ of p53 ubiquitination of newly synthesized compounds 1–6

Compound	Description	IC ₅₀ (μM) of p53 ubiquitination <i>in vitro</i>	IC ₅₀ (μM) of p53 ubiquitination <i>in vivo</i>
1	Ligand	1.24	12.13
2	Mn(II) complex	0.35	2.89
3	Co(II) complex	0.73	6.35
4	Ni(II) complex	0.65	5.27
5	Cu(II) complex	0.21	1.79
6	Zn(II) complex	0.16	1.44
	4,5-Diphenylimidazole	0.26	1.88

promising inhibitor activity compared with the positive control (IC₅₀ = 0.26 μM). The inhibitor activity of the compounds for p53 ubiquitination can be arranged in descending order as follows: zinc complex > copper complex > manganese complex > nickel complex > cobalt complex > ligand. It is noticeable that the inhibitor activity of ligand **1** increases through coordination with metal ions, which may be due to chelation changing the properties of the ligand, like conductivity, solubility and dipole moment. Moreover, the complexes may deactivate various cellular enzymes, which have an essential role in various metabolic pathways.^[63] There is a need for further biological studies to help us understand the mechanisms of operation of the newly synthesized compounds for inhibition of p53 ubiquitination. This may open the way for the generation of more chemotherapeutic agents targeting the ubiquitination of the p53 system in the future.

4 | CONCLUSIONS

A series of metal complexes of a new chromone Schiff base have been prepared. Analytical and spectroscopic studies have characterized the structure of the novel compounds, where the chromone Schiff base ligand coordinates with metal ions through deprotonated hydroxyl group, carbonyl oxygen atom of antipyrine moiety and azomethine nitrogen atom. All these complexes exhibit a distorted octahedral geometry except the nickel complex, which displays a tetrahedral geometry. All the complexes have a non-electrolytic nature. The newly synthesized compounds show potent inhibitor activity for p53 ubiquitination compared with a standard drug. These promising results especially for zinc and copper complexes make it possible for their use as new p53 activators after studying the mechanism of their action.

ORCID

Mohamad M.E. Shakdofa  <http://orcid.org/0000-0003-0399-1658>

Hanan A. Mousa  <http://orcid.org/0000-0001-6373-4552>
 Ammar A. Labib  <http://orcid.org/0000-0002-1564-3477>
 Amira S. Abd-El-All  <http://orcid.org/0000-0002-3271-8426>
 Ahmed A. El-Beih  <http://orcid.org/0000-0002-6960-027X>

REFERENCES

- [1] E. Middleton Jr., C. Kandaswami, T. C. Theoharides, *Pharmacol. Rev.* **2000**, *52*, 673.
- [2] A. Pick, H. Müller, R. Mayer, B. Haenisch, I. K. Pajeva, M. Weigt, H. Bönisch, C. E. Müller, M. Wiese, *Bioorg. Med. Chem.* **2011**, *19*, 2090.
- [3] G. Peterson, S. Barnes, *Biochem. Biophys. Res. Commun.* **1991**, *179*, 661.
- [4] A. A. el-Gammal, R. M. Mansour, *Zentralbl. Mikrobiol.* **1986**, *141*, 561.
- [5] J. B. Harborne, C. A. Williams, *Phytochemistry* **2000**, *55*, 481.
- [6] T. P. T. Cushnie, A. J. Lamb, *Int. J. Antimicrob. Agents* **2005**, *26*, 343.
- [7] G. Atassi, P. Briet, J. J. Berthelon, F. Collonges, *Eur. J. Med. Chem.* **1985**, *20*, 393.
- [8] J. B. Harborne, *The Flavonoids: Advances in Research Since*, Vol. 1986, Chapman and Hall, London **1995**.
- [9] S. Amaral, L. Mira, J. M. F. Nogueira, A. P. da Silva, M. H. Florêncio, *Bioorg. Med. Chem.* **2009**, *17*, 1876.
- [10] Z. Nowakowska, *Eur. J. Med. Chem.* **2007**, *42*, 125.
- [11] D. Yu, A. Brossi, N. Kilgore, C. Wild, G. Allaway, K. H. Lee, *Bioorg. Med. Chem. Lett.* **2003**, *13*, 1575.
- [12] P. B. Kaufman, J. A. Duke, H. Brielmann, J. Boik, J. E. Hoyt, *J. Altern. Complement. Med.* **1997**, *3*, 7.
- [13] C. H. Fanta, *New Engl. J. Med.* **2009**, *360*, 1002.
- [14] A. Kandil, W. Gobran, H. A. Samaan, H. Abu Shady, *J. Drug Res.* **1977**, *9*, 35.
- [15] M. Himaja, K. Rai, K. V. Anish, M. V. Ramana, A. A. Karigar, *J. Pharm. Sci. Inn.* **2012**, *1*, 67.
- [16] S. Sigroha, B. Narasimhan, P. Kumar, A. Khatkar, K. Ramasamy, V. Mani, R. K. Mishra, A. B. A. Majeed, *Med. Chem. Res.* **2012**, *21*, 3863.
- [17] Y. K. Vaghasiya, R. Nair, M. Soni, S. Baluja, S. Chanda, *J. Serb. Chem. Soc.* **2004**, *69*, 991.

- [18] S. Bondock, R. Rabie, H. A. Etman, A. A. Fadda, *Eur. J. Med. Chem.* **2008**, *43*, 2122.
- [19] M. A. Metwally, M. A. Gouda, A. N. Harmal, A. M. Khalil, *Eur. J. Med. Chem.* **2012**, *56*, 254.
- [20] Y. Kakiuchi, N. Sasaki, M. Satoh-Masuoka, H. Murofushi, K. Murakami-Murofushi, *Biochem. Biophys. Res. Commun.* **2004**, *320*, 1351.
- [21] T. Rosu, M. Negoiu, S. Pasculescu, E. Pahontu, D. Poirier, A. Gulea, *Eur. J. Med. Chem.* **2010**, *45*, 774.
- [22] D. Burdulene, A. Palaima, Z. Stumbryavichyute, *Pharm. Chem. J.* **1999**, *33*, 191.
- [23] G. Turan-Zitouni, M. Sivaci, F. S. Kiliç, K. Erol, *Eur. J. Med. Chem.* **2001**, *36*, 685.
- [24] M. S. Alam, J. H. Choi, D. U. Lee, *Bioorg. Med. Chem.* **2012**, *20*, 4103.
- [25] P. M. P. Santos, A. M. M. Antunes, J. Noronha, E. Fernandes, A. J. S. C. Vieira, *Eur. J. Med. Chem.* **2010**, *45*, 2258.
- [26] A. N. Lutsevich, K. I. Bender, O. V. Reshet'ko, *Eksp. Klin. Farmakol.* **1995**, *58*, 51.
- [27] N. V. Chandrasekharan, H. Dai, K. L. T. Roos, N. K. Evanson, J. Tomsik, T. S. Elton, D. L. Simmons, *Proc. Natl Acad. Sci. USA* **2002**, *99*, 13926.
- [28] M. M. Abd-Elzaher, S. A. Moustafa, A. A. Labib, H. A. Mousa, M. M. Ali, A. E. Mahmoud, *Appl. Organometal. Chem.* **2012**, *26*, 230.
- [29] M. M. Abd-Elzaher, S. A. Moustafa, H. A. Mousa, A. A. Labib, *Monatsh. Chem.* **2012**, *143*, 909.
- [30] M. F. R. Fouda, M. M. Abd-Elzaher, M. M. Shakdofa, F. A. El-Saied, M. I. Ayad, A. S. El Tabl, *J. Coord. Chem* **2008**, *61*, 1983.
- [31] M. F. R. Fouda, M. M. Abd-Elzaher, M. M. E. Shakdofa, F. A. El Saied, M. I. Ayad, A. S. El Tabl, *Transit. Met. Chem.* **2008**, *33*, 219.
- [32] F. A. El-Saied, M. M. E. Shakdofa, A. S. El-Tabl, M. M. A. Abd-Elzaher, *Main Group Chem.* **2014**, *13*, 87.
- [33] F. A. El Saied, M. M. Abd-Elzaher, A. S. El Tabl, M. M. E. Shakdofa, A. J. Rasras, *Beni-suef Univ. J. Basic Appl. Sci.* **2017**, *6*, 24.
- [34] L. Lewis, R. G. Wilkins, *Modern Coordination Chemistry*, Interscience, New York **1960**.
- [35] N. J. Marston, T. Crook, K. H. Vousden, *Oncogene* **1994**, *9*, 2707.
- [36] J. Chen, J. Lin, A. J. Levine, *Mol. Med.* **1995**, *1*, 142.
- [37] O. E. Sherif, N. S. Abdel-Kader, *Spectrochim. Acta A* **2014**, *117*, 519.
- [38] N. Beyazit, B. Çatıkkaş, Ş. Bayraktar, C. Demetgül, *J. Mol. Struct.* **2016**, *1119*, 124.
- [39] A. L. El-Ansary, H. M. Abdel-Fattah, N. S. Abdel-Kader, *J. Coord. Chem.* **2008**, *61*, 2950.
- [40] A. Kulkarni, S. A. Patil, P. S. Badami, *Eur. J. Med. Chem.* **2009**, *44*, 2904.
- [41] R. M. Amin, N. S. Abdel-Kader, A. L. El-Ansary, *Spectrochim. Acta A* **2012**, *95*, 517.
- [42] R. C. Maurya, S. Rajput, *J. Mol. Struct.* **2007**, *833*, 133.
- [43] A. K. El-Sawaf, F. El-Essawy, A. A. Nassar, E.-S. A. El-Samanody, *J. Mol. Struct.* **2018**, *1157*, 381.
- [44] A. S. El-Tabl, *Transit. Met. Chem.* **2002**, *27*, 166.
- [45] K. Nakamoto, *Infrared and Raman Spectra of Inorganic and Coordination Compounds Part B: Applications in Coordination, Organometallic, and Bioinorganic Chemistry*, John Wiley, Hoboken, NJ **2009**.
- [46] A. H. F. Abd El-Wahab, H. M. Mohamed, A. M. El-Agrody, M. A. El-Nassag, A. H. Bedair, *Lett. Org. Chem.* **2012**, *9*, 360.
- [47] W. J. Geary, *Coord. Chem. Rev.* **1971**, *7*, 81.
- [48] A. B. P. Lever, *Inorganic Electronic Spectroscopy*, Elsevier Science, Amsterdam **1984**.
- [49] S. Xiao-Hui, Y. Xiao-Zeng, L. Cun, X. Ren-Gen, Y. Kai-Be, *Transit. Met. Chem.* **1995**, *20*, 191.
- [50] S. Chandra, A. Kumar, *Spectrochim. Acta A* **2007**, *68*, 1410.
- [51] S. Chandra, S. Sharma, *Transit. Met. Chem.* **2007**, *32*, 150.
- [52] A. S. El-Tabl, R. M. El-Bahnasawy, M. M. E. Shakdofa, A. E. D. A. Ibrahim Hamdy, *J. Chem. Res.* **2010**, 88.
- [53] A. N. M. A. Alaghaz, H. A. Bayoumi, Y. A. Ammar, S. A. Aldhlmani, *J. Mol. Struct.* **2013**, *1035*, 383.
- [54] S. Chandra, L. K. Gupta, *Spectrochim. Acta A* **2004**, *60*, 1563.
- [55] S. Chandra, S. Gautam, H. K. Rajor, R. Bhatia, *Spectrochim. Acta A* **2015**, *137*, 749.
- [56] A. A. El-Bindary, A. Z. El-Sonbati, *Pol. J. Chem.* **2000**, *74*, 615.
- [57] T. Rosu, E. Pahontu, C. Maxim, R. Georgescu, N. Stanica, G. L. Almajan, A. Gulea, *Polyhedron* **2010**, *29*, 757.
- [58] Y. Yang, C.-C. H. Li, A. M. Weissman, *Oncogene* **2004**, *23*, 2096.
- [59] P. Roxburgh, A. K. Hock, M. P. Dickens, M. Mezna, P. M. Fischer, K. H. Vousden, *Carcinogenesis* **2012**, *33*, 791.
- [60] I. V. Davydov, D. Woods, Y. J. Safiran, P. Oberoi, H. O. Fearnhead, S. Fang, J. P. Jensen, A. M. Weissman, J. H. Kenten, K. H. Vousden, *J. Biomol. Screen.* **2004**, *9*, 695.
- [61] K. H. Vousden, D. P. Lane, *Nat. Rev. Mol. Cell Biol.* **2007**, *8*, 275.
- [62] C. A. Midgley, C. J. Fisher, J. Bartek, B. Vojtesek, D. Lane, D. M. Barnes, *J. Cell Sci.* **1992**, *101*, 183.
- [63] R. S. Joseyphus, M. S. Nair, *Mycobiology* **2008**, *36*, 93.

How to cite this article: Shakdofa MME, Mousa HA, Labib AA, Abd-El-All AS, El-Beih AA, Abdalla MM. Synthesis and characterization of novel chromone Schiff base complexes as p53 activators. *Appl Organometal Chem.* 2018;e4345. <https://doi.org/10.1002/aoc.4345>